INFLUENCE OF SURFACE AND PROCESS INDUCED DEFECTS ON POTENTIAL-INDUCED DEGRADATION AND REGENERATION

A. Schütt, J. Carstensen, J.-M. Wagner, H. Föll
Institute for Materials Science, Faculty of Engineering, Christian-Albrechts-University of Kiel,
Kaiserstr. 2, 24143 Kiel, Germany, email: jc@tf.uni-kiel.de, Phone: (+49) 431 880 6181, Fax: (+49) 431 880 6178

ABSTRACT: It is well known that the composition of the silicon nitride AR coating as well as the choice of the EVA foil drastically influence potential-induced degradation (PID). In this paper experimental results are presented and discussed indicating that the lamination process itself and the surface topology of the solar cell can enhance PID as well. A model allowing to explain the experimental results is proposed indicating some concepts to prevent PID.

Keywords: Module characterization, CELLO, PID, regeneration

1 INTRODUCTION

Module performance may fall victim to Potential Induced Degradation (PID). It has been observed that the choice of the modules EVA foil as well as the quality of the silicon nitride anti-reflection (AR) coating may drastically influence the appearance of PID. Microscopic models based on TEM analysis propose [1, 2] that a reverse bias applied across the dielectric silicon nitride (as AR coating) leads to an electrical-field-driven transport of sodium ions through the nitride layer. This seems to be the crucial step to introduce sodium into the emitter and thus leading to shunts, because a better conductive nitride layer does not show the accumulation of sodium ions at the nitride emitter interface and consequently no PID. In this paper we present results that the lamination process itself and the surface topology of the solar cell can enhance PID. Combining our experimental results with the microscopic model outlined above a model is proposed which allows to suggest some concepts to prevent PID.

2 EXPERIMENTAL DETAILS

2.1 Module production, PID formation, and regeneration procedures

A set of 5 industrial multicrystalline (mc) Si solar cells, known to exhibit possibly PID due to their SiN deposition parameters, is processed to single-cell modules (i.e. stringing, EVA encapsulation, cover glass, back sheet). These modules are PID-degraded and PID-regenerated. PID has been generated by applying 1000 V between the wet module glass surface and the module terminals for 168 hours. The regeneration is the same process but with –1000 V applied instead.

2.2 Measurements

For each step (cell as such, module, degradation, regeneration) the set of solar cells has been fully electrically analyzed using the CELLO technique [3 - 7] in order to quantify local losses in the cell performance (roughly 100 maps have been measured). For all measurements a laser wavelength of 650 nm has been used.

In addition the global *I–V* curves at 1/3 sun have been measured and the shunt resistance has been obtained from fitting these curves.

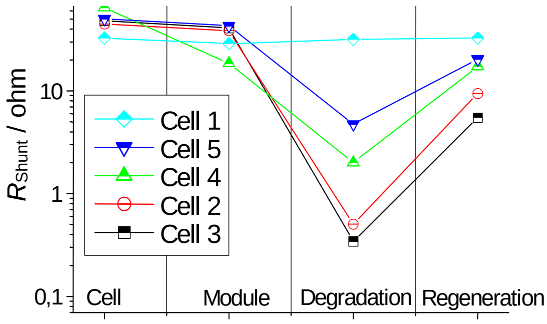

Figure 1: Global R_{shunt} of *I–V* curve fit at 1/3 sun reveal the PID behavior.

3 RESULTS AND DISCUSSION

3.1 Degradation phenomena

The global R_{shunt} values of 5 samples have been calculated by fitting the *I–V* curve under 1/3 sun illumination (see Fig. 1). Already on some cells a slight decrease of the shunt resistivity is found just after module fabrication. The origin of this degradation will be discussed using the CELLO results and it can be clearly distinguished from the severe degradation phenomena found after applying the high voltage to induce PID. Different degrees of PID are found already from the integral shunt values. Remarkably, no full regeneration is found on these samples although a quite long recovery time was chosen. Not all data are shown here due to lack of space but there is very good agreement between the overall area in the CELLO maps showing strong losses and the (inverse of the) global shunt resistance.

All CELLO maps discussed here give information about the shunt positions, but do not scale directly with their strengths. As an example Fig. 2 shows results for one of the two cells with the strongest PID. a) and b) are ratio maps between voltage at open circuit and short circuit current maps. This ratio shows losses in forward direction (e.g. bad diodes, high series resistance) as dark areas [4]. While before module fabrication only material-induced losses due to dislocation-rich areas and grain boundaries are visible in Fig. 2a), additional series resistance losses are visible after module fabrication in Fig. 2b). These series resistance losses have been identified by optical microscope inspection through the module glass as due to grid fingers disconnected from the main bus bar by the soldering process [cf. Fig. 2d), A].

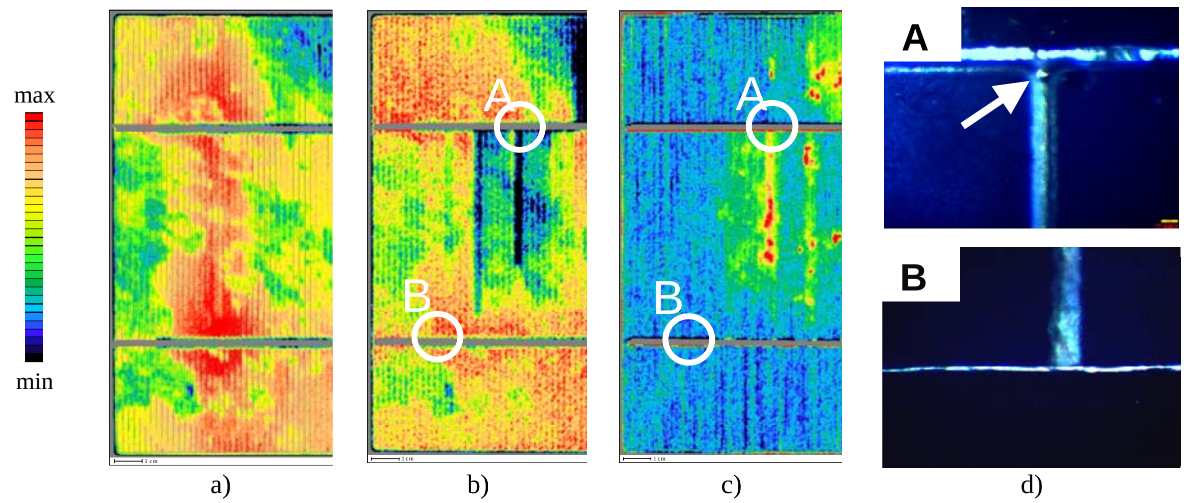

Figure 2: Ratio of CELLO maps of cell #2 with strong PID. a) Before (voltage map at open circuit divided by current map at short circuit), b) after module fabrication (voltage map at open circuit divided by current map at short circuit), c) after PID (photo-current map at –300 mV cell bias divided by short-circuit current map). d) Optical microscope images through the module glass of areas A and B marked in c), where single grid fingers reach at the bus bar. The color scale bar shown at the far left holds for all CELLO maps.

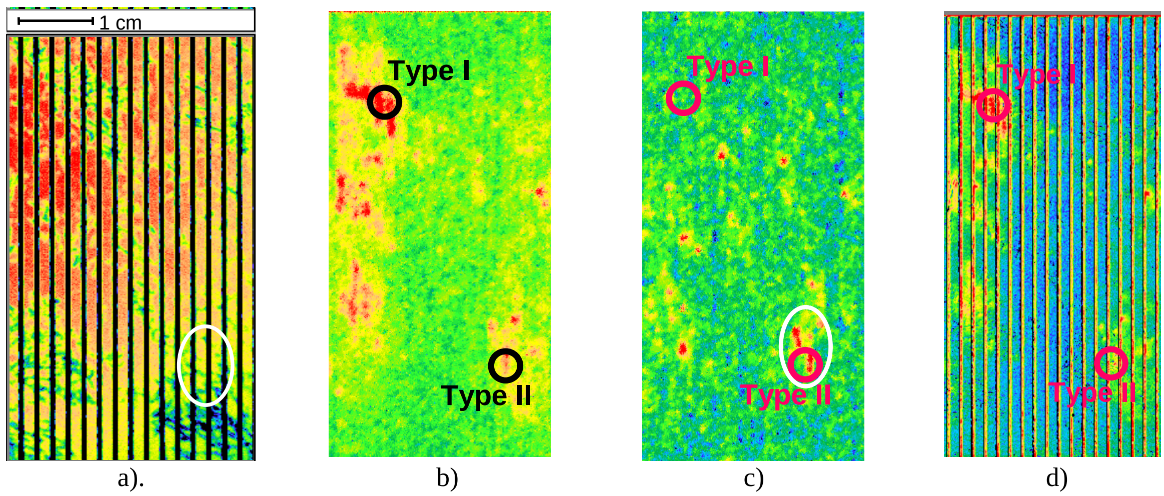

Figure 3: CELLO maps of cell #3 with strong PID. a) Short-circuit current after module fabrication. b), c) Ratio of two CELLO photo-current maps (–300 mV divided by short circuit), b) before and c) after regeneration, red areas indicate regions of strong PID. d) Ratio of CELLO photo-current maps at –300 mV before regeneration divided by after regeneration, red areas indicate regions of significant improvement of cell performance.

Figure 2c) shows results for the same area after PID generation; it is a ratio map between photo-current under reverse bias divided by the short-circuit current map. This ratio map is the standard CELLO map to identify the position of shunts [3]; it is not sensitive to series resistance losses. In Fig. 2c), PID losses show up in red colors. Although a certain correlation is found between Fig. 2b) and Fig. 2c) we do not believe that PID is directly related to series resistance losses, as will be discussed later.

Figure 3 shows CELLO maps for cell #3 which according to the integral data exhibits PID most strongly. This cell did not show any artifacts of the module fabrication, which is already a first hint that series resistance problems are not a decisive feature of PID on the solar cells under investigation. Due to the missing of fabrication artifacts of disconnected grid fingers this cell has been chosen for the investigation of material-related PID effects. Figure 3b) indicates in red areas strong PID. Comparing with the short-circuit map, Fig. 3a), a certain correlation to areas with high dislocation density is found. Again we do not believe that PID is directly related to the recombination activity but via a more indirect effect of recombination-active regions in mc-Si, as will be discussed below.

It is quite obvious that nearly all areas showing PID are oriented parallel to the grid fingers. The magnification of these images allows to identify the PID areas to be arranged not symmetrically around a grid finger (which would be the case if series resistance problems, e.g. induced by broken grid fingers, would cause PID) but always lying between grid fingers, i.e. a grid finger always limits the area of PID. Actually this is true for all PID areas on cell #2 in Fig. 2c) as well.

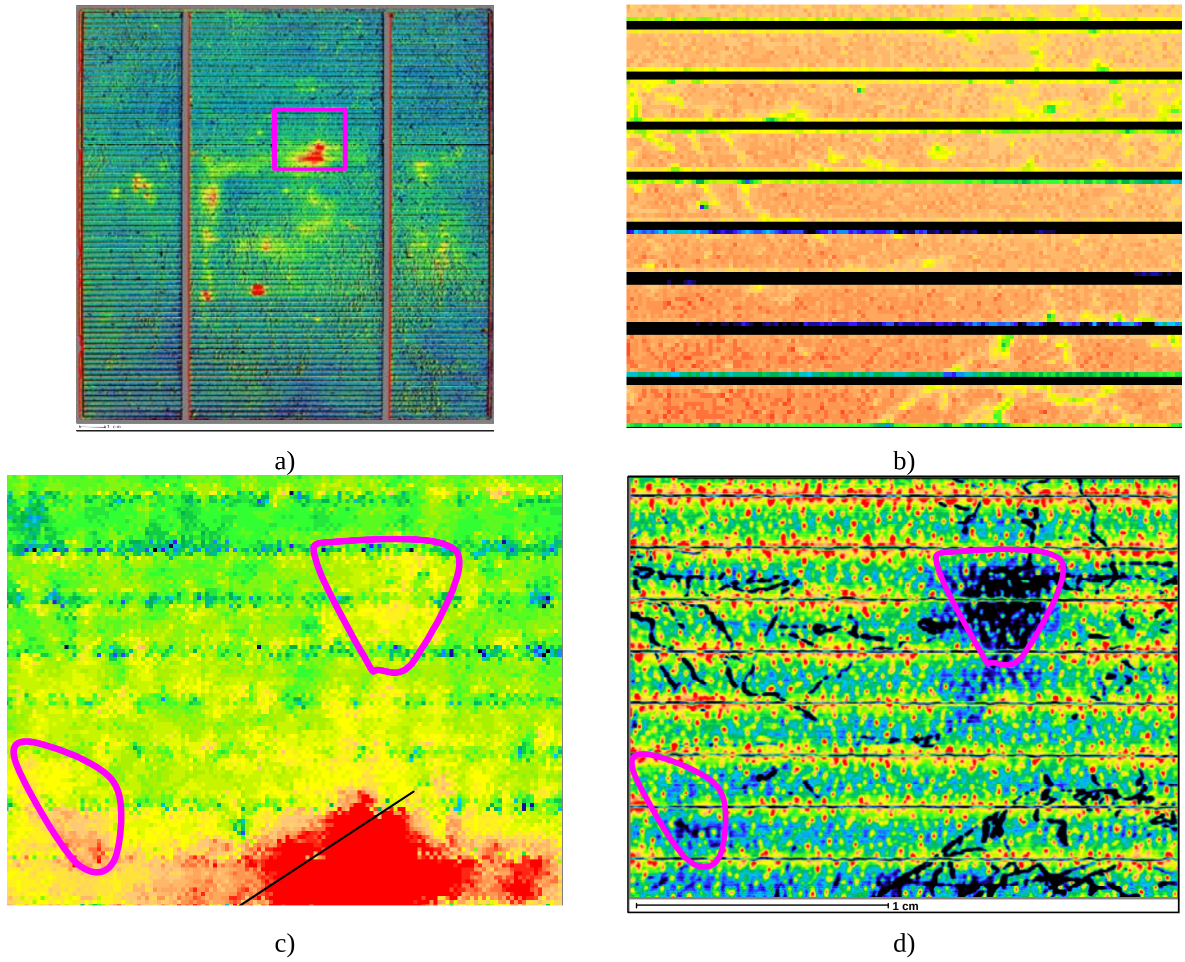

Figure 4: CELLO maps of cell #4 with strong PID. Ratio of short-circuit current map before divided by short-circuit current map after degradation, with PID-affected areas in red: a) complete cell and c) zoom of area marked in a), the black line in c) being a guide to the eye (see text). d) Short-circuit current map of the same area of the module after regeneration. b) For comparison, short-circuit current map taken on the cell as such (before module fabrication) for the same area as in d).

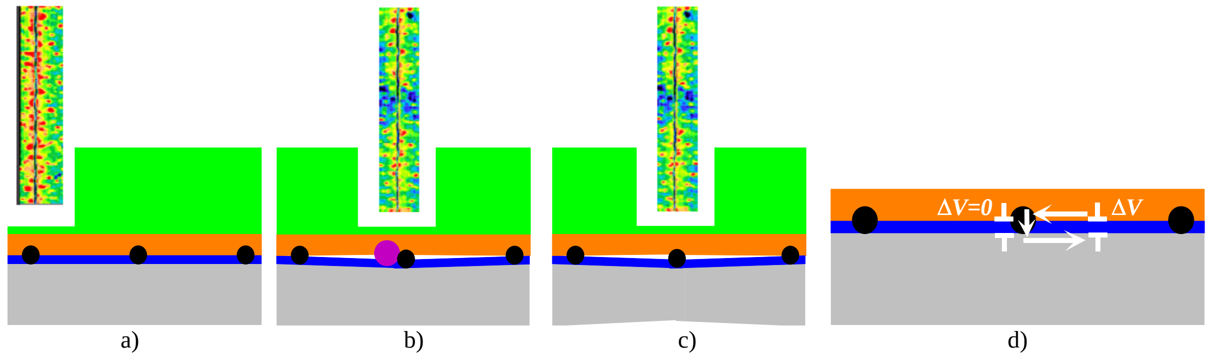

Figure 5: Illustration of the sandwich structure of glass (green), EVA foil (orange), grid finger (black), SiN (blue) and Si (grey). a) Normal case with sufficient EVA–SiN contact, b) and c) defected EVA–SiN contact caused by different local lamination pressures induced by particle inclusion (b) or reduced cell thickness (c). Above in a)–c): CELLO map according to Fig. 4d) corresponding to the grid finger below. d) The voltage drop ΔV over the SiN is reduced to 0 V at the grid fingers.

Figure 3c) marks all areas in red which could not be regenerated on cell #2. Here a strict correlation to areas with grain boundaries (cf. Fig. 3a) is found. Such occurrences of PID we named type-II. Typically these areas are small and spherically, the position is not related to grid fingers since, as already mentioned, they are always located at grain boundaries. Most PID areas, however, have completely different properties; therefore we named them type-I. They are often limited by grid fingers, therefore often have an elongated shape and they can be regenerated to a large extent.

Figure 4a) shows the PID areas of cell #4 in red. Most of them are found in two elongated areas oriented perpendicular to each other, one parallel to the main bus bars and one parallel to the grid fingers. Quite obviously these structures are related to the fabrication process. The area marked by the rectangle in Fig. 4a) has been remeasured with a higher spatial resolution; results are shown in Fig. 4c) and 4d). Figure 4d) is a short-circuit current map of the solar cell under encapsulation, taken after regeneration. The red dots, most prominently visible in this map, have never been observed on solar cells without EVA and glass encapsulation. As an example Fig. 4b) presents the short-circuit current map of the same area for the solar cell without encapsulation, taken by the same laser with a somewhat larger focus size (which is not relevant for this comparison) than in Fig. 4d), showing the typical, much more homogeneous local photo-current of the solar cell as such.

Obviously the density of red dots in Fig. 4d) is much higher close to grid fingers. We are quite sure that the density of the red dots reflects the pressure by which the EVA foil is pressed to the solar cell. Probably due to the intrinsic roughness of the EVA foil the optical transparency increases when the contact to the solar cell is more intimate. Figure 4c) shows the same ratio map as Fig. 4a), scaled slightly differently to make the nearly perfect anticorrelation between the density of red dots in Fig. 4d) and the strength of PID more obvious (cf. the areas marked in Fig. 4c, d). According to this observation most of the PID on this solar cell is induced by a fabrication-related non-perfect contact of the EVA foil to the solar cell.

For the worst PID in the lower right part of Fig. 4c) the reason is most probably a combination of fabrication and material defects. As a guide to the eye the position of a prominent grain boundary visible in Fig. 4d) is marked in Fig. 4c) by a black line. One boundary of the PID area is nearly perfectly parallel to this grain boundary, but they do not coincide. It is well known that different grains as well as dislocation-rich areas in mc-Si solar cells can lead to different cell thicknesses after the polishing etch step always used at the beginning of the cell fabrication. The enhanced chemical dissolution rate typically found in regions with increased bulk recombination, leading to thinner areas on the solar cell, may explain why the contact of the EVA foil to the solar cell is even worse in this region. The same explanation may hold for the PID areas in Fig. 3b) marked as type-I.

A similar explanation may hold for the solar cell shown in Fig. 2. Here most PID areas are close to the upper main bus bar. In addition to some disconnected grid fingers the optical microscope analysis showed some artifacts related to the soldering process. The white spot marked by the arrow in Fig. 2d), part A, is an elevated metal particle soldered to the main bus bar not allowing the module glass to press the EVA foil homogenously onto the solar cell in this area.

Figure 5a) summarizes the experimental findings which may lead to a "gap" between EVA foil and solar cell, which is found as a possible reason for PID. This can be monitored by the density of red dots as shown in Fig. 4d): The high density of red dots around the two grid fingers in the uppermost part of Fig. 4d) may be interpreted as a nearly perfect sealing of the area between the two grid fingers. If (as has been proposed earlier) water vapor is incorporated into the PID formation scheme [8] this nearly perfect sealing could limit the transport of vapor into the solar cell to the area between two grid fingers and thus limit PID formation to this area. This could explain the elongated shape and the limitation by grid fingers found for nearly all PID areas in this investigation.

An even more simple model could explain all our experimental findings. It does not need any further assumptions like the incorporation of water vapor but just uses the ingredients already mentioned in the introduction of a voltage drop across the dielectric AR coating layer of roughly 5 V which drives sodium ions through this layer. Since an ohmic contact is generated by firing the metallization of the grid fingers through the AR coating into the emitter, no voltage drop across the AR coating can exist directly below the grid fingers, i.e. no PID should be possible there according to the explanation given here. If a lateral sodium ion transport through the EVA foil is easier than through the dielectric AR coating layer, an intimate contact of the EVA foil both to the grid fingers and the area between the grid fingers may help to reduce the voltage drop necessary to drive PID. This is schematically illustrated in Fig. 5d). Of course any conducting layer at the top of the AR coating may do the same job, so to overcome PID it would not be necessary to increase the conductivity of the whole AR coating layer which has drawbacks for the optical properties of the AR coating.

4 CONCLUSION

PID-affected areas have been found to lie in between grid fingers. There are large type-I areas with nearly complete regeneration; most PID-affected areas are of this type. There are much smaller type-II areas with a nearly spot-like occurrence of PID which cannot be completely regenerated. All type-II spots found in this investigation are located at grain boundaries.

There is a general correlation between PID-affected areas and areas of reduced mechanical contact between EVA foil and SiN layer as observed from CELLO short-circuit current maps measured at the module or from optical microscope investigation through the module glass. Such reduced mechanical contact between EVA foil and SiN layer can be due to particle inclusion or locally reduced cell thickness (e.g. in regions with high dislocation densities).

Altogether, these findings show (i) that the lamination process itself can enhance PID in areas where it results in a non-perfect contact of the EVA foil to the solar cell and (ii) that this can be influenced by the surface topology of the solar cell, which in some areas is related to the material properties.

A model for the (non-)occurrence of PID is proposed that considers the consequences of the voltage drop across the AR coating, necessary to drive the shunt-creating sodium ions through the AR coating, being shorted at the grid fingers; this model can consistently explain all experimental findings of this investigation.

5 ACKNOWLEDGEMENTS

This work was supported by the Deutsche Forschungsgemeinschaft under grant No. FO 285/11-2.

6 REFERENCES

[1] V. Naumann, D. Lausch, A. Graff, M. Werner, S. Swatek, J. Bauer, A. Hähnel, O. Breitenstein, S. Großer, J. Bagdahn, C. Hagendorf, *Phys. Status Solidi RRL* **7(5)**, 315 (2013).

[2] V. Naumann, D. Lausch, A. Hähnel, J. Bauer, O. Breitenstein, A. Graff, M. Werner, S. Swatek, S. Großer, J. Bagdahn, C. Hagendorf, *Sol. Energy Mater. Sol. Cells*, DOI: 10.1016/j.solmat.2013.06.015 (2013).

[3] J. Carstensen, G. Popkirov, J. Bahr, H. Föll, *Sol. Energy Mater. Sol. Cells* **76**, 599 (2003).

[4] J. Carstensen, S. Mathijssen, G. Popkirov, H. Föll, in *Proc. 20th European Photovoltaic Solar Energy Conference*, 1AV.2.40, Barcelona (2005).

[5] J. Carstensen, A. Schütt, H. Föll, in *Proc. 22nd European Photovoltaic Solar Energy Conference*, 1CV.1.34, Milan (2007).

[6] J. Carstensen, A. Schütt, H. Föll, in *Proc. 23rd European Photovoltaic Solar Energy Conference*, 1CV.1.38, Valencia (2008).

[7] J. Carstensen, A. Schütt, G. Popkirov, H. Föll, *Phys. Status Solidi C* **8(4)**, 1342 (2011).

[8] S. Hoffmann, M. Koehl, *Prog. Photovolt: Res. Appl.*, DOI: 10.1002/pip.2238 (2012).